Low density instabilities in asymmetric nuclear matter within the quark-meson coupling (QMC) model with the δ meson

Alexandre M. Santos and Constança Providência
Centro de Física Computacional, Department of Physics, University of Coimbra, P-3004-516 Coimbra, Portugal

Prafulla K. Panda
Indian Association for the Cultivation of Science, Jadavpur, Kolkata-700 032, India and
Centro de Física Computacional, Department of Physics, University of Coimbra, P-3004-516 Coimbra, Portugal

(Received 19 January 2009; published 13 April 2009)

In the present work we include the isovector-scalar δ meson in the quark-meson coupling (QMC) model and study the properties of asymmetric nuclear within QMC without and with the δ meson. Recent constraints set by isospin diffusion on the slope parameter of the nuclear symmetry energy at saturation density are used to adjust the model parameters. The thermodynamical spinodal surfaces are obtained and the instability region at subsaturation densities within QMC and QMCδ models are compared with mean-field relativistic models. The distillation effect in the QMC model is discussed.

DOI: 10.1103/PhysRevC.79.045805 PACS number(s): 21.65.−f, 21.30.−x, 95.30.Tg

I. INTRODUCTION

The instabilities presented by a system are directly related with the possible phase transitions it can undertake. At subsaturation densities a liquid-gas phase transition in nuclear matter is predicted and it is normally tested in nuclear reactions. The formation of highly excited composed nuclei in equilibrium with a gas of evaporated particles can be interpreted in the framework of hydrodynamics as two coexisting phases of nuclear matter, a liquid and a gas phase. During these reactions, phase transitions may occur depending on the temperature and densities involved. The liquid-gas phase transition also plays an important role in the description of the crust of compact star matter at densities between 0.03 fm^{-3} and saturation density ($\sim$0.15 fm^{-3}). It essentially consists of neutron-rich nuclei immersed in a gas of neutrons. It has been shown that this phase transition leads to an isospin distillation phenomenon: the isospin content of each phase is different, most of the gas being composed of neutrons and the liquid being closer to symmetric matter [1].

In the present article, we employ the quark-meson coupling (QMC) model [2,3] to investigate the thermodynamical instabilities of asymmetric nuclear matter (ANM). In the QMC model, nuclear matter is described as a system of nonoverlapping MIT bags that interact through the exchange of scalar and vector mean fields. An earlier study of ANM within this model has been focused on the effect of isospin asymmetry and temperature on the equation of state and on the coexistence surface [4]. We here consider an extension of the model that includes the scalar isovector virtual $\delta[a_0(980)]$ field [5]. Its presence introduces in the isovector channel the structure of relativistic interactions, where a balance between a scalar (attractive) and a vector (repulsive) potential exists. The δ and ρ mesons give rise to the corresponding attractive and repulsive potentials in the isovector channel. The introduction of the δ meson will affect the behavior of the system at both low and high densities. In the last case due to Lorentz contraction, its contribution is reduced, leading to a harder equation of state (EOS) at densities larger than $\sim 1.5\rho_0$ [6]. At low densities a reduction of the symmetry energy will occur that will allow for more asymmetric matter.

In Refs. [7,8] the instabilities in ANM have been investigated within relativistic mean-field hadron models, both with constant and density-dependent couplings at zero and finite temperatures. It was shown that the main differences occur at large isospin asymmetry and at finite temperature. In particular it has been shown that the predicted density at the inner edge of the crust of a compact star, from the crossing of the β-equilibrium EOS, is model dependent [9].

In the present work we investigate thermodynamical instabilities within the QMC model with and without the isovector-scalar δ meson. Although in this model the isoscalar vector channel described by the ρ meson is included in a similar way to the nonlinear Walecka model (NLWM), the nonlinearities in the σ and δ fields arise from the minimization of the bag energy. In particular, the NLWM used in Ref. [5] does not include nonlinearities in the δ meson. We may therefore expect a different behavior of asymmetric matter.

The article is organized as follows: in Sec. II an extension of the QMC model to include the δ meson is discussed, in Sec. III we make a short review of the calculation of the spinodal surface, in Sec. IV results are presented and discussed, and some conclusions are drawn in the last section.

II. THE QUARK-MESON COUPLING MODEL

In what follows we present a review of the QMC model and its generalization to include the isovector-scalar δ meson.

In the QMC model, the nucleon in nuclear medium is assumed to be a static spherical MIT bag in which quarks interact with the scalar (σ, δ) and vector (ω, ρ) fields, and those are treated as classical fields in the mean-field approximation (MFA) [2,3]. The quark field, ψ_{q_i}, inside the bag then satisfies

the equation of motion:

$$\left[i\partial\!\!\!/ - \left(m_q^0 - g_\sigma^q\sigma - g_\delta^q\tau_z\delta_3\right) - g_\omega^q\omega\gamma^0 + \tfrac{1}{2}g_\rho^q\tau_z\rho_{03}\gamma^0\right] \times \psi_{q_i}(x) = 0, \quad q = u, d, \tag{1}$$

where m_q^0 is the current quark mass and g_σ^q, g_δ^q, g_ω^q, and g_ρ^q denote the quark-meson coupling constants. The normalized ground state for a quark in the bag is given by

$$\psi_{q_i}(\mathbf{r},\mathbf{t}) = \mathcal{N}_{q_i}\exp(-i\epsilon_{q_i}t/R_i) \times \begin{bmatrix} j_{0_i}\left(x_{q_i}r/R_i\right) \\ i\beta_{q_i}\vec{\sigma}\cdot\hat{r}\,j_{1_i}\left(x_{q_i}r/R_i\right) \end{bmatrix}\frac{\chi_q}{\sqrt{4\pi}}, \tag{2}$$

where

$$\epsilon_{q_i} = \Omega_{q_i} + R_i\left(g_\omega^q\omega + \frac{1}{2}g_\rho^q\tau_z\rho_{03}\right); \qquad \beta_{q_i} = \sqrt{\frac{\Omega_{q_i} - R_i m_q^*}{\Omega_{q_i} + R_i m_q^*}}, \tag{3}$$

with the normalization factor given by

$$\mathcal{N}_{q_i}^{-2} = 2R_i^3 j_0^2(x_q)[\Omega_q(\Omega_q - 1) + R_i m_q^*/2]/x_q^2, \tag{4}$$

where $\Omega_{q_i} \equiv \sqrt{x_{q_i}^2 + (R_i m_q^*)^2}$, $m_q^* = m_q^0 - g_\sigma^q\sigma - g_\delta^q\tau_z\delta_3$, R_i is the bag radius of nucleon i and χ_q is the quark spinor. The bag eigenvalue for nucleon i, x_{q_i}, is determined by the boundary condition at the bag surface

$$j_{0_i}(x_{q_i}) = \beta_{q_i} j_{1_i}(x_{q_i}). \tag{5}$$

The energy of a static bag describing nucleon i consisting of three quarks in ground state is expressed as

$$E_i^{\text{bag}} = \sum_q n_q\frac{\Omega_{q_i}}{R_i} - \frac{Z_i}{R_i} + \frac{4}{3}\pi R_i^3 B_N, \tag{6}$$

where Z_i is a parameter that accounts for zero-point motion of nucleon i and B_N is the bag constant. The set of parameters used in the present work is given in Ref. [10]. The effective mass of a nucleon bag at rest is taken to be $M_i^* = E_i^{\text{bag}}$. The equilibrium condition for the bag is obtained by minimizing the effective mass, M_i^*, with respect to the bag radius

$$\frac{dM_i^*}{dR_i^*} = 0, \quad i = p, n. \tag{7}$$

The total energy density of the nuclear matter reads

$$\varepsilon = \frac{1}{2}m_\sigma^2\sigma^2 + \frac{1}{2}m_\omega^2\omega_0^2 + \frac{1}{2}m_\rho^2\rho_{03}^2 + \frac{1}{2}m_\delta^2\delta_3^2 + \sum_N\frac{1}{\pi^2}\int_0^{k_N}k^2dk\left[k^2 + M_N^{*2}(\sigma,\delta)\right]^{1/2} \tag{8}$$

and the free energy density is given by

$$\mathcal{F} = \varepsilon - \mu_p\rho_p - \mu_n\rho_n,$$

where the chemical potentials are given by

$$\mu_p = \sqrt{k_p^2 + M_p^{*2}} + g_\omega\rho + \frac{g_\rho}{2}\rho_{03},$$
$$\mu_n = \sqrt{k_p^2 + M_n^{*2}} + g_\omega\rho - \frac{g_\rho}{2}\rho_{03}.$$

The vector mean field ω_0 and ρ_{03} are determined through

$$\omega_0 = \frac{g_\omega(\rho_p + \rho_n)}{m_\omega^2}, \quad \rho_{03} = \frac{g_\rho(\rho_p - \rho_n)}{m_\rho^2}, \tag{9}$$

where $g_\omega = 3g_\omega^q$ and $g_\rho = g_\rho^q$. Finally, the mean fields σ_0 and δ_3 are fixed by

$$\frac{\partial\varepsilon}{\partial\sigma} = 0, \quad \frac{\partial\varepsilon}{\partial\delta_3} = 0. \tag{10}$$

To set the model parameters, we start by fixing the free space bag properties. They are obtained by fitting the nucleon mass and enforcing the stability condition for the bag in free space. We consider two sets of free space parameters, taking an equal proton and neutron mass value in a first moment and then proceeding by considering different proton and neutron masses after.

In the first case, we consider the bare nucleon mass $M = 939$ MeV and the bag radius, $R_p = R_n = 0.6$ fm. The unknowns $Z_p = Z_n = 3.986991$ and $B_N^{1/4} = 211.30305$ MeV are then obtained by setting the nucleon bag energies to that (single) bare nucleon mass value.

In the next step, we take the physical nucleon mass values as $M_p = 938.272$ MeV and $M_n = 939.56533$ MeV and the bag radius for protons as $R_p = 0.6$ fm. The unknowns $Z_p = 3.98865$, $Z_n = 3.98471$, $B_N^{1/4} = 211.26209$ MeV, and the neutron radius $R_n = 0.6002$ are then obtained. Note that for fixed proton bag radius $R_p = 0.6$ we observe a decrease on Z_n and on the bag parameter $B_N^{1/4}$ for the nucleons. Next, we fit the quark-meson coupling constants g_σ^q, g_δ^q, $g_\omega = 3g_\omega^q$ and $g_\rho = g_\rho^q$ for the nucleons to obtain the correct saturation properties of nuclear matter, $E_N \equiv \epsilon/\rho - M = -15.7$ MeV at $\rho = \rho_0 = 0.15$ fm^{-3}, $a_{\text{sym}} = 33.7$ MeV. For the couplings, we have $g_\sigma^q = 5.981$, $g_\omega = 8.954$. In our first case (when no effective mass difference between p, n is considered), $g_\rho = 8.615$.

The properties of asymmetric nuclear matter have recently been related to both terrestrial data and star properties from Vela pulsar glitches, which sets the symmetry energy slope value to $L = 88 \pm 25$ MeV [11,12]. We then consider the δ meson and determine the values of the couplings so as to have $L = 102.077$ MeV, which sets $g_{\rho N} = 12.599$ and $g_\delta^q = 12.6$. In this case, the (p, n) mass splitting manifests in the different values for the effective masses: $M_p^* = 727.718$ MeV and $M_n^* = 729.007$ MeV, at saturation.

We take the standard values for the meson masses, namely $m_\sigma = 550$ MeV, $m_\omega = 783$ MeV, and $m_\rho = 770$ MeV.

III. STABILITY CONDITIONS

The stability conditions for asymmetric nuclear matter, keeping constant volume and temperature are obtained from the free energy density $\mathcal{F}$, imposing that this function is a convex function of the densities ρ_p and ρ_n, i.e., the symmetric matrix with elements

$$\mathcal{F}_{ij} = \left(\frac{\partial^2\mathcal{F}}{\partial\rho_i\partial\rho_j}\right)_T, \tag{11}$$

is positive [13–15]. This is equivalent to imposing

$$\frac{\partial \mu_p}{\partial \rho_p} > 0, \quad \frac{\partial(\mu_p, \mu_n)}{\partial(\rho_p, \rho_n)} > 0, \tag{12}$$

where we have used $\mu_i = \left.\frac{\partial \mathcal{F}}{\partial \rho_i}\right|_{T, \rho_{j\neq i}}$.

The two eigenvalues of the stability matrix are given by [15]

$$\lambda_\pm = \frac{1}{2}[\mathrm{Tr}(\mathcal{F}) \pm \sqrt{\mathrm{Tr}(\mathcal{F})^2 - 4\mathrm{Det}(\mathcal{F})}], \tag{13}$$

and the eigenvectors $\delta\rho_\pm$ by

$$\frac{\delta\rho_i^\pm}{\delta\rho_j^\pm} = \frac{\lambda_\pm - \mathcal{F}_{jj}}{\mathcal{F}_{ji}}, \quad i, j = p, n.$$

The largest eigenvalue is always positive, whereas the other can take on negative values. We are interested in the latter, as it defines the spinodal surface, which is determined by the values of T, ρ, and y_p for which the smallest eigenvalue of $\mathcal{F}_{ij}$ becomes negative. The associated eigenvector defines the instability direction of the system, in isospin space.

It has recently been argued [14] that in ANM the spinodal instabilities cannot be separately classified as mechanical or chemical instabilities. In fact, the two conditions that give rise to the instability of the system are coupled so that the instability appears as an admixture of nucleon density and concentration fluctuations. In the following we study the direction of instability and the spinodal for the different models considered.

IV. RESULTS AND DISCUSSIONS

In the present section we compare the model properties of QMC and QMCδ, respectively, with and without the δ meson, the nonlinear Walecka model (NLWM) NL3 [16], with and without the δ meson, and the density-dependent relativistic hadron model TW [17]. We will also refer to the nuclear matter properties obtained within a microscopic Brueckner-Hartree-Fock (BHF) approximation using the realistic Argonne V18 nucleon-nucleon potential plus a three-body force of Urbana type [18].

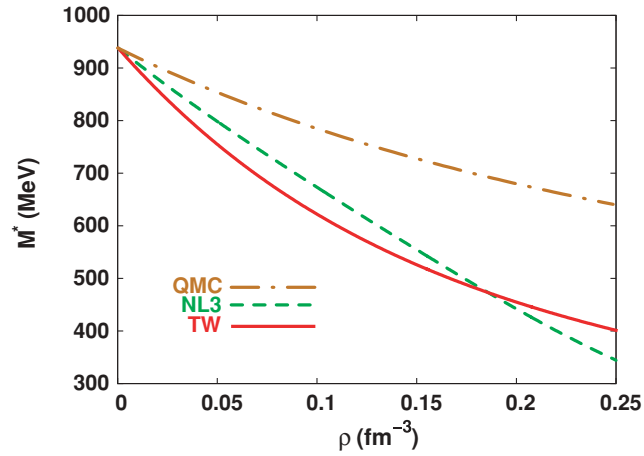

FIG. 1. (Color online) Effective mass for QMC (brown, dot-dashed), NL3 (green, dashed), and TW (red) in symmetric matter.

A. Model properties

We will first compare the equilibrium properties of nuclear matter described by the different models considered. The parameters of these models have been fitted to similar binding energy and saturation density values as seen in Table I. At saturation, the effective mass in QMC is much larger than the corresponding mass in the other models, which is a characteristic of the model [3]. In Fig. 1, it is seen that the QMC mass decreases much slower with density. Even the hadronic models we study show quite different behavior among themselves. NL3 has an almost linear decrease on the mass whereas TW has much faster drop at low densities, and shows a less dramatic fall as density increases, crossing the curve for NL3 at $\rho \sim 0.18$ fm^{-3}. Incompressibility is one of the bulk properties that distinguishes the different models, but it is on the isovector channel that lies the largest distinctions among the different models we use. Although having identical (or barely different) values for their bulk isoscalar properties, similar models differ considerably on the isovector parameters we discuss next.

We now compare the symmetry energy and its slope and compressibility for all models in this work (Fig. 2 and Table I). The symmetry energy in our relativistic mean-field

TABLE I. Nuclear matter properties of the models used in the present work. All quantities are taken at saturation, except the density ρ_s for which the pressure has a minimum and the incompressibility is zero. In the relativistic models the effective mass should be identified with the Dirac mass while for BHF it is the Landau mass.

Model	B/A (MeV)	ρ_0 (fm^{-3})	K (MeV)	M^*/M	$\mathcal{E}_{\mathrm{sym}}$ (MeV)	L (MeV)	K_{sym} (MeV)	K_{asy} (MeV)	ρ_s (fm^{-3})
NL3 [16]	16.3	0.148	269	0.60	37.4	118.3	101	−608.8	0.096
NL3δ	16.3	0.148	270	0.60	37.4	153.1	427.1	−491.5	0.096
TW [17]	16.3	0.153	240	0.56	32.0	55.3	−125	−456.8	0.096
QMC	15.7	0.150	291	0.77	33.7	93.5	−10	−570.8	0.098
QMCδ	15.7	0.150	291	0.77	34.2	102.1	34.8	−577.6	0.098
BHF [18]	14.7	0.182	176.5	0.79	33.2	63.4	6.04	−374.3	0.119

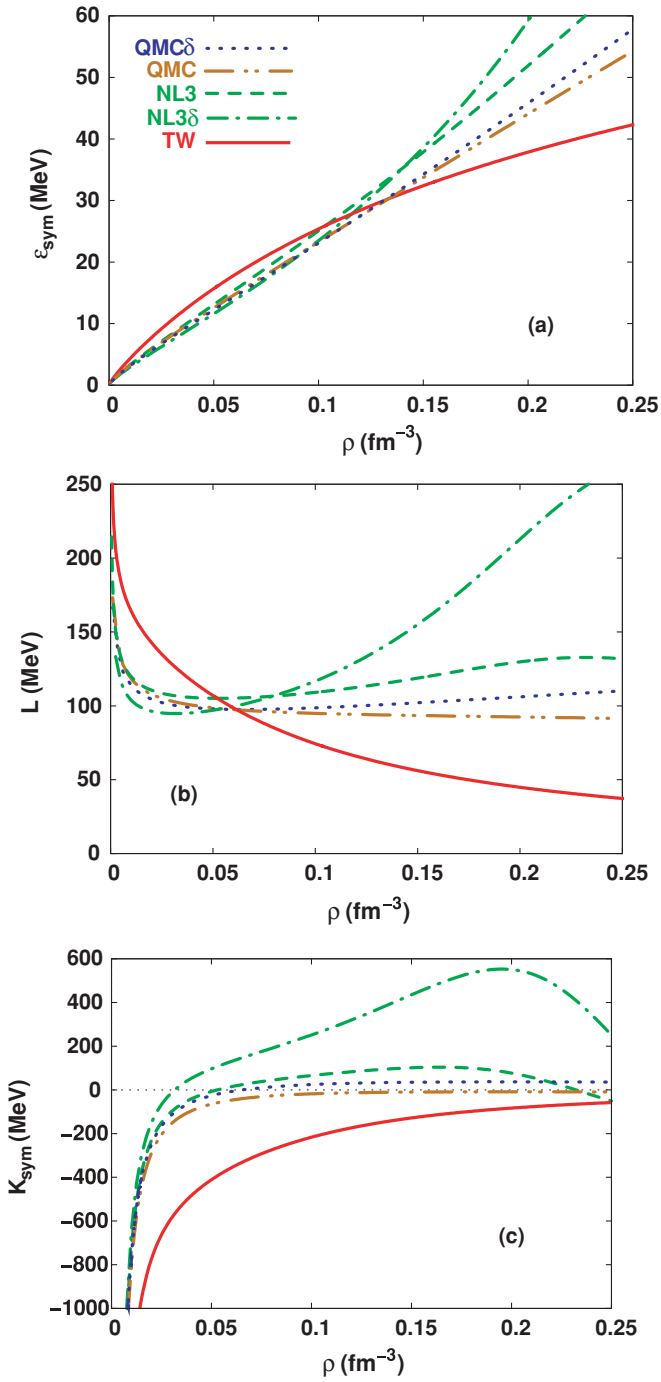

FIG. 2. (Color online) Symmetry energy (a) and its slope parameter $L = 3\rho_0 \mathcal{E}'_{\rm sym}$ (b) and $K_{\rm sym}$ (c) in the QMCδ (blue, dotted), QMC (brown, dot-dot-dashed), NL3 (dark green, dashed), NL3δ (light green, dot-dashed), and TW (red) models for symmetric matter.

models is given by

$$\mathcal{E}_{\rm sym} = \frac{{k_F}^2}{6{\epsilon_F}^2} + \frac{\rho}{2}\left[\frac{g_\rho^2}{4m_\rho^2} - \frac{g_\delta^2}{m_\delta^2}\left(\frac{M_0^*}{\epsilon_F}\right)^2\right], \qquad (14)$$

where $\epsilon_F = \sqrt{P_F^2 + M_0^{*2}}$ is the Fermi energy of the nucleons and M_0^* is their effective mass in symmetric matter. The NL3 models have the largest value at saturation of the models considered, 37.4 MeV.

The symmetry energy slope $L(\rho)$ is defined by $L = 3\rho_0 \partial \mathcal{E}_{\rm sym}/\partial\rho$. The curvature parameter of the symmetry energy $K_{\rm sym} = 9\rho_0^2 \partial^2 \mathcal{E}_{\rm sym}/\partial\rho^2$ [Fig. 2(c)] is also of interest because it distinguishes between different parametrizations. In particular, the quantity $K_{\rm asy} = K_{\rm sym} - 6L$ can be directly extracted from measurements of the isotopic dependence of the giant monopole resonance (GMR) [19]. Recent measurements of the GMR on even-A Sn isotopes give a quite stringent value of $K_{\rm asy} = -550 \pm 100$ MeV. According to this value, the hadronic and QMC models we use here (see Table I) satisfy the above constraint, whereas the BHF results lie slightly below.

The symmetry energy within QMC and QMCδ shows an extremely linear behavior with density [Fig. 2(a)], in comparison with all hadron models shown. This is quite visible from the symmetry energy curves but undoubtedly clear from the slope parameter L [Fig. 2(b)]. At larger densities the symmetry energy in QMC is essentially defined by the second term of Eq. (14), proportional to the density, due to the small variation of the nucleon effective mass with density. Although still quite hard above saturation density, the QMC symmetry energy is softer than NL3 but harder than TW. At subsaturation densities and considering only models without the δ meson, the QMC symmetry energy takes the smallest values. The introduction of the δ has the expected effect: at subsaturation densities the symmetry energy is softer but above saturation values it becomes harder due to the saturation of the δ-meson field [5]. In Fig. 2 we show both the NL3δ and QMCδ symmetry energies. The effect of the δ meson on the QMC at subsaturation densities is quite small, much smaller than the effect seen in NL3. It is above the saturation density that the δ meson has a larger effect in QMC. From the slope of the symmetry energy it is seen that although for QMC the slope decreases slightly with density, for the QMCδ model it increases slightly, with a value close to 100 MeV. In the bottom figure we also plot $K_{\rm sym}$. The δ has a very strong effect in the NL3 model. The QMC model is less affected but in both cases the presence of the δ increases the symmetry incompressibility $K_{\rm sym}$, becoming slightly positive for QMCδ while it was slightly negative for QMC. The model TW is presenting the smallest values.

Figure 3 shows the proton and neutron radii for proton fractions $y_p = 0.5$ and 0.0. For symmetric matter, the neutron bag is larger in this model due to the mass proton-neutron difference. This result has also been reported in Ref. [3]. Decreasing the proton fraction increases the proton radius and the neutron and proton radii cross at a certain value of the density, isospin dependent: density: $\sim$0.175 fm^{-3} for $y_p = 0.3$, $\sim$ 0.11 fm^{-3} for $y_p = 0.1$, and $\sim$0.1 fm^{-3} for neutron matter. The bag radius is sensitive to isospin content by a small amount. It is, however, quite clear from the neutron matter results ($y_p = 0.0$) that the isospin contents of the nucleons leads to higher radii differences at higher densities. Moreover, proton bags become larger than neutrons in medium, as matter goes denser. The neutron radius does not change much with isospin and for symmetric matter and neutron matter QMC and QMCδ neutron radii almost overlap.

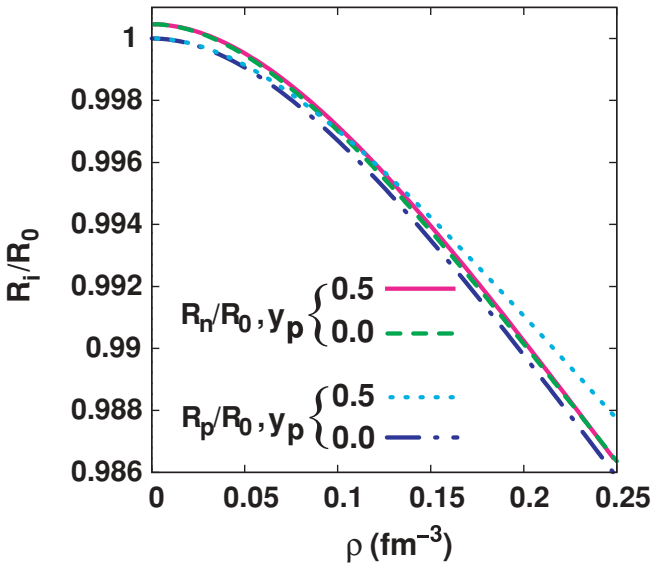

FIG. 3. (Color online) Radii ratios for neutron and proton, for symmetric matter and for $y_p = 0.0$ in the QMCδ model. Here we have taken $R = 0.6$ fm^{-3}.

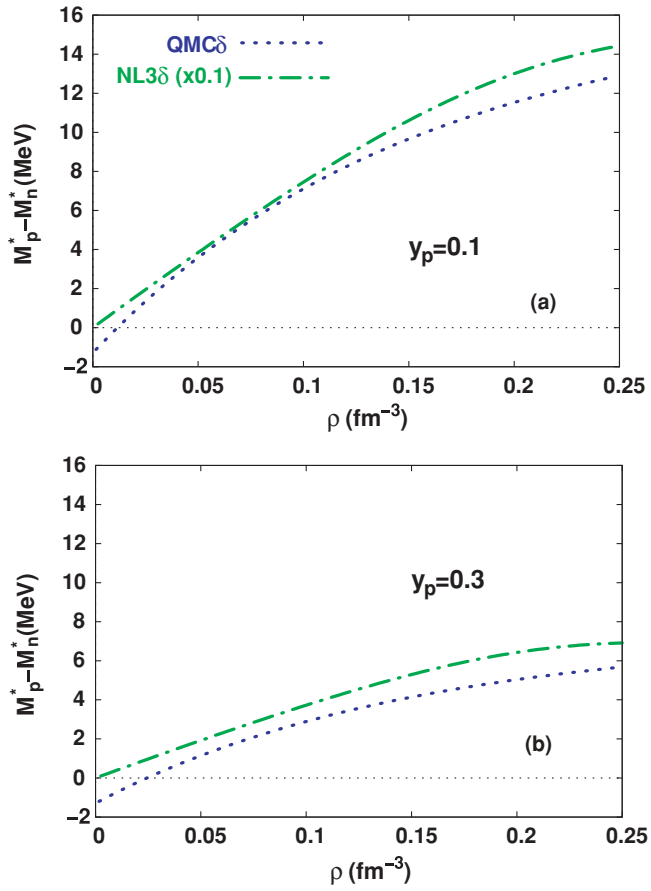

FIG. 4. (Color online) Effective mass differences $M_p - M_n$, for QMCδ (blue, dotted) and NL3δ (light green, dot-dashed), for different proton fractions: $y_p = 0.1$ (a) and $y_p = 0.3$ (b). Note that the values for NL3δ have been scaled by a 0.1 factor.

In Fig. 4 we show the effective mass difference $M_p^* - M_n^*$ for both QMCδ and NL3δ, for $y_p = 0.3$ and 0.1. For NL3, we show the mass difference multiplied by a factor of 0.1 to compare with QMCδ. The most striking result is the factor of 10 difference between the p, n mass splitting in NL3 and QMC. In both models, this effect increases with baryon density, but it is worth remarking that the effective mass is larger for neutrons than for protons at lower densities, which is represented by the negative values in the figures. As referred to before, this occurs because the proton and neutron masses were considered different at zero density. In addition, for the same proton fraction, the crossing of the p, n effective mass curves (equal effective p, n masses) does not occur for the same densities as the proton and neutron radius, R_p and R_n (Fig. 3)

The effect of the δ meson is to increase the $M_p^* - M_n^*$ difference as it occurs in NL3δ and other relativistic mean-field (RMF) models. In Ref. [20] the authors give a thorough discussion of the effect of the δ meson on the effective mass, identified as a Dirac mass. When a comparison is made with nonrelativistic models it is important that the same definition of effective masses is used, namely, instead of the Dirac mass, the Schrödinger mass should be evoked. In Ref. [21] it was shown that for RMF models, the Schrödinger mass of neutrons is smaller than the corresponding proton mass for neutron-rich matter, in contrast with the Dirac-Brueckner-Hartree-Fock results or the Brueckner-Hartree-Fock calculations [22,23] that predict a larger neutron effective mass, understood as a Landau mass in the nonrelativistic approach.

We have computed the Schrödinger effective masses (see Eq. 6.35 of Ref. [20]) for QMC and verified that in neutron-rich matter the neutron mass is smaller than the proton one just like the Dirac mass and in other relativistic mean-field models.

B. Instabilities

In the present subsection we discuss the results for the instability region at subsaturation densities with QMC, QMCδ, and the hadron models we have considered. In Fig. 5 we plot the spinodal curves for np matter. As referred to before, they are defined by the points, for a given temperature, density, and

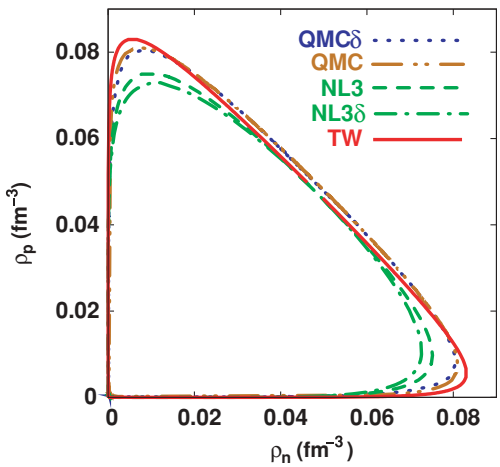

FIG. 5. (Color online) Spinodal (thermodynamical instability border) for QMC, QMCδ, NL3, NL3δ and TW.

isospin asymmetry, that make the curvature matrix of the free energy vanish.

Both QMC and QMCδ present larger instability regions than NL3, NL3δ, and TW on the isoscalar direction, $\rho_p = \rho_n$. This is possibly due to the σ contribution in the Lagrangian for QMC (both with and without δ): the fields here attain magnitudes to minimize the bag energy, whereas in hadron models their mean-field values are determined by solving the relevant set of equations where nonlinearities show explicitly or through density-dependent couplings. The extension of the spinodal for $\rho_p = \rho_n$ defines the density ρ_s, corresponding to the density value for which the pressure of symmetric nuclear matter has a minimum and the incompressibility is zero [24]. We have included the values of this density for the different models in Table I. Recently [18] it was shown that within a Brueckner-Hartree-Fock calculation the isoscalar extension of the spinodal was much larger than NLWM and Skyrme interaction predictions.

For large isospin asymmetries the presence of δ reduces the instability region both in QMC and NL3. NL3 has a higher symmetry energy than NL3δ for densities ranging from 0 up to $\sim\rho_0$, and the same occurs for QMC although the differences are smaller. This means that highly asymmetric matter is less bound in NL3 and QMC than in NL3δ and QMCδ. A mere inspection of the symmetry energy is not enough to account for the differences in the instability region if different models are considered [24]. With the introduction of the δ meson the scalar channel is not affected, and therefore we are essentially changing the isovector channel. We also notice that at $\rho_p = \rho_n$ the curvature of the QMC spinodal is intermediate between NL3 and TW. As shown in Ref. [24] this curvature is defined by the symmetry energy and its first and second derivatives.

The nuclear liquid-gas coexistence phase is characterized by different isospin contents for each phase, i.e., the clusterized regions are more isospin symmetric than the surrounding nuclear gas, the so-called isospin distillation [11,25]. The extension of the distillation effect is model dependent and it has been shown that NL3 and other NLWM parametrizations lead to larger distillation effects than the density-dependent hadron models [6,8,24]. However, the distillation effect was also studied within a BHF calculation [18] and a smaller distillation effect was generally obtained.

In Fig. 6 we show the ratio of the proton versus the neutron density fluctuations corresponding to the unstable mode. This ratio defines the direction of instability of the system. We show the results for different proton fractions (including rather small values), for the sake of studying the effectiveness of the models in restoring the symmetry in the liquid phase.

We first compare the three models not including the δ meson: QMC, NL3, and TW. We see that QMC has a behavior which is intermediate between NL3 and TW. The distillation effect for densities above 0.02 fm^{-3} is larger than the prediction of TW, but for the larger densities it also shows a tendency to decrease, contrary to NL3. The presence of δ meson makes the distillation effect more efficient.

In Fig. 7 we plot the proton-neutron density fluctuation ratio as a function of the isospin asymmetry for a fixed nuclear density, $\rho = 0.06$ fm^{-3}. We compare all models under study, NL3, NL3δ, TW, QMC, and QMCδ, and include also the

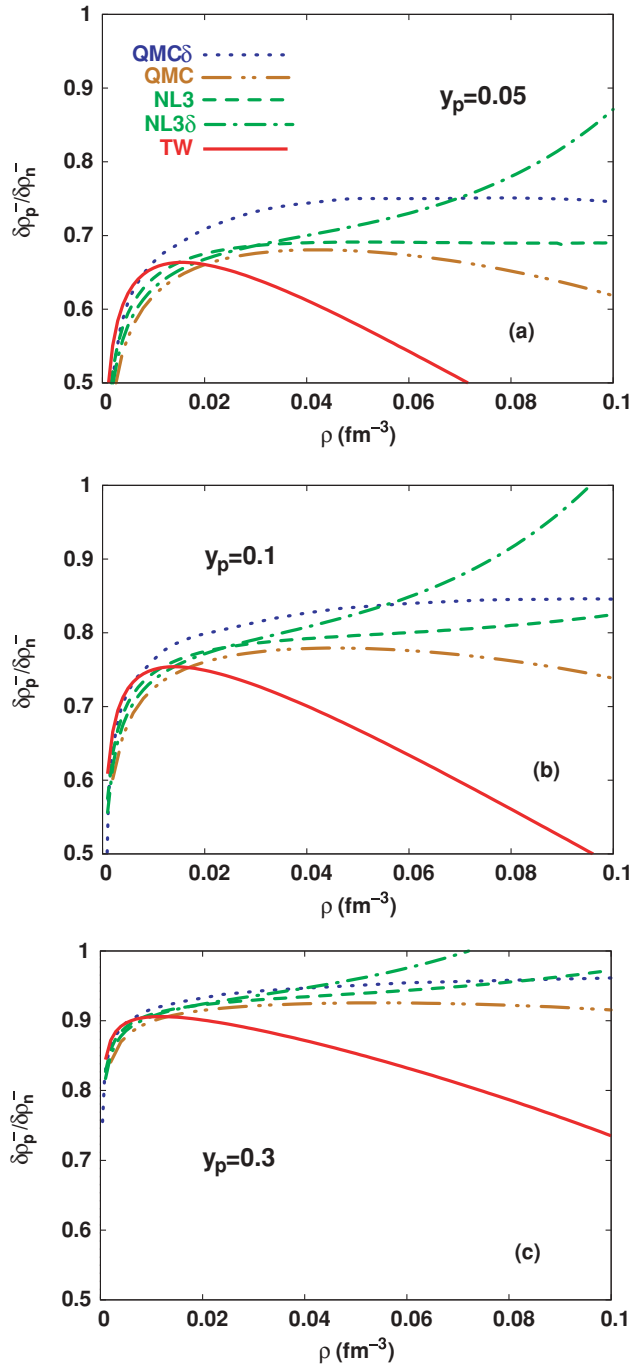

FIG. 6. (Color online) Direction of instability (eigenvector for negative eigenvalue λ_-) for $y_p = 0.05$ (a), 0.1 (b), and 0.3 (c).

results derived from the BHF approach [18] referred above. All the relativistic models predict larger fluctuation ratios than the corresponding value of ρ_p/ρ_n, dotted line. The behavior gives rise to a distillation effect, which, as referred before, is larger for NL3 and smaller for TW, with QMC presenting intermediate values. The δ meson stresses the distillation effect, clearly seen both in QMCδ and NL3δ.

However, except for the very asymmetric matter ($y_p < 0.02$), both QMC and the other relativistic models predict fluctuations with larger proton fractions than BHF. The

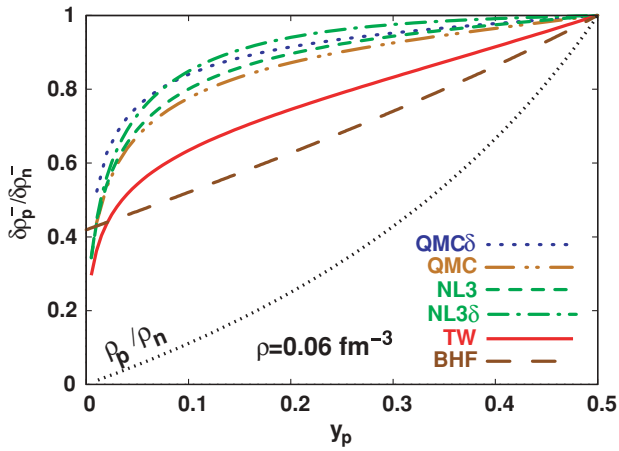

FIG. 7. (Color online) Proton-neutron density fluctuation ratio versus the isospin asymmetry for a fixed nuclear density, $\rho = 0.06$ fm^{-3}. The BHF results were obtained by Vidaña and Polls [18].

instability properties within the BFH calculation of Ref. [18] show also differences for the spinodal surface: the unstable region is larger, extending to larger densities both in the isoscalar an isovector directions and the curvature of the spinodal at $\rho_p = \rho_n$ is much larger than the one of all the relativistic models considered. A larger extension of the unstable region is justified because the saturation density is larger, 0.182 fm^{-3}. The shape of the spinodal itself depends on the density dependence of the symmetry energy and its derivatives. It would be important to identify the properties that define the shape of the spinodal for the more asymmetric matter.

We have studied subsaturation nuclear instabilities for both symmetric and asymmetric matter within the QMC model, with and without the inclusion of the δ meson. In this model the nucleons are described as nonoverlapping bags. We propose a parametrization for QMCδ with a the symmetry energy slope value $L = 102$ MeV within the interval $L = 88 \pm 25$ MeV proposed in Refs. [11,12] and that was determined from nuclear laboratory data. It was interesting to notice that for QMC and QMCδ the quantity $K_{\rm asy}$ defined in Ref. [11], and which can be directly extracted from measurements of the isotopic dependence of the giant monopole resonances, falls inside the interval predicted by experiments. The BHF calculation predicts a value of $K_{\rm asy}$ that is not very far, though lower than the interval obtained from GMR, $K_{\rm asy} = 550 \pm 100$ MeV.

A comparison was done with the results obtained from a NLWM parametrization (NL3), one density-dependent relativistic model (TW), along with BHF with the Argonne V18 potential calculation. It was shown that the restoration of isospin symmetry, obtained by a distillation effect, was more efficient in QMC with respect to TW but less efficient when compared with NL3. The spinodal surface within QMC is closer to TW although with a larger curvature at $\rho_p = \rho_n$ and a slightly smaller instability extension at larger asymmetries, while the inclusion of the δ meson (QMCδ) shrinks the asymmetric parts of the instability envelope. The BHF results of Ref. [18], although with similar general properties, differ in the extension and shape of the spinodal and in the amount of distillation predicted.

A study of the QMC instability properties at finite temperatures is now under preparation, as well as a more detailed study of the isospin dependence of Schrödinger effective mass in our approach. It is also important to identify how the density dependence of the symmetry energy determines the shape of the spinodal for large isospin asymmetries.

ACKNOWLEDGMENTS

This work was partially supported by FEDER and FCT (Portugal) under the projects POCI/FP/81923/2007, CERN/FP/83505/2008 and SFRH/BPD/29057/2006. The authors acknowledge I. Vidaña for kindly providing us with some data for comparison in this work.

[1] H. S. Xu *et al.*, Phys. Rev. Lett. **85**, 716 (2000).
[2] P. A. M. Guichon, Phys. Lett. **B200**, 235 (1988).
[3] K. Saito and A. W. Thomas, Phys. Lett. **B327**, 9 (1994); **B335**, 17 (1994); **B363**, 157 (1995); Phys. Rev. C **52**, 2789 (1995); P. A. M. Guichon, K. Saito, E. Rodionov, and A. W. Thomas, Nucl. Phys. **A601**, 349 (1996); K. Saito, K. Tsushima, and A. W. Thomas, *ibid.* **A609**, 339 (1996); Phys. Rev. C **55**, 2637 (1997); Phys. Lett. **B406**, 287 (1997); P. K. Panda, A. Mishra, J. M. Eisenberg, and W. Greiner, Phys. Rev. C **56**, 3134 (1997); P. K. Panda, D. P. Menezes, and C. Providência, *ibid.* **69**, 025207 (2004).
[4] P. K. Panda, G. Krein, D. P. Menezes, and C. Providência, Phys. Rev. C **68**, 015201 (2003).
[5] B. Liu, V. Greco, V. Baran, M. Colonna, and M. Di Toro, Phys. Rev. C **65**, 045201 (2002).
[6] Constança Providência, Int. J. Mod. Phys. E **16**, 2680 (2007).
[7] S. S. Avancini, L. Brito, D. P. Menezes, and C. Providência, Phys. Rev. C **70**, 015203 (2004).
[8] S. S. Avancini, L. Brito, Ph. Chomaz, D. P. Menezes, and C. Providência, Phys. Rev. C **74** 024317 (2006).
[9] S. S. Avancini, D. P. Menezes, M. D. Alloy, J. R. Marinelli, M. M. W. Moraes, and C. Providencia, Phys. Rev. C **78**, 015802 (2008).
[10] P. K. Panda, D. P. Menezes, and C. Providência, Phys. Rev. C **69**, 025207 (2004).
[11] J. Xu, L. W. Chen, B. A. Li, and H. R. Ma, Phys. Rev. C **77**, 014302 (2008).
[12] J. Xu, L. W. Chen, B. A. Li, and H. R. Ma, Phys. Rev. C **79**, 035802 (2009).
[13] V. Baran, M. Colonna, M. Di Toro, and A. B. Larionov, Nucl. Phys. **A632**, 287 (1998).
[14] J. Margueron and P. Chomaz, Phys. Rev. C **67**, 041602(R) (2003); P. Chomaz, M. Colonna, and J. Randrup, Phys. Rep. **389**, 263 (2004).
[15] H. Müller and B. D. Serot, Phys. Rev. C **52**, 2072 (1995).
[16] G. A. Lalazissis, J. König, and P. Ring, Phys. Rev. C **55**, 540 (1997).

[17] S. Typel and H. H. Wolter, Nucl. Phys. **A656**, 331 (1999).
[18] I. Vidaña and A. Polls, Phys. Lett. **B666**, 232 (2008).
[19] Bao-An Li, Lie-Wen Chen, and Che Ming Ko, Phys. Rep. **464**, 113 (2008).
[20] V. Baran, M. Colonna, V. Greco, and M. Di Toro, Phys. Rep. **410**, 335 (2005).
[21] E. N. E. van Dalen, C. Fuchs, and Armand Faessler, Phys. Rev. Lett. **95**, 022302 (2005).
[22] C. Fuchs and H. H. Wolter, Eur. Phys. J. A **30**, 5 (2006).
[23] W. Zuo, A. Lejeune, U. Lombardo, and J. F. Mathiot, Nucl. Phys. **A706**, 418 (2002); T. Frick, Kh. Gad, H. Muther, and P. Czerski, Phys. Rev. C **65**, 034321 (2002).
[24] C. Ducoin, C. Providência, A. M. Santos, L. Brito, and Ph. Chomaz, Phys. Rev. C **78**, 055801 (2008).
[25] Ph. Chomaz, Nucl. Phys. **A685**, 274c (2001).